Title

Hydrogen isotope analysis in W-tiles using fs-LIBS

Journal

Scientific Reports, 13(1)

ISSN

2045-2322

Authors

Mittelmann, Steffen
Touchet, Kévin
Mao, Xianglei
et al.

Publication Date

2023

DOI

10.1038/s41598-023-29138-2

Peer reviewed

scientific reports

Check for updates

OPEN

Hydrogen isotope analysis in W-tiles using fs-LIBS

Steffen Mittelmann[1]✉, Kévin Touchet[2], Xianglei Mao[2], Minok Park[2], Sebastijan Brezinsek[3], Georg Pretzler[1] & Vassilia Zorba[2,4]

Laser-Induced Breakdown Spectroscopy (LIBS) is a promising technology for in-situ analysis of Plasma-Facing Components in magnetic confinement fusion facilities. It is of major interest to monitor the hydrogen isotope retention i.e. tritium and deuterium over many operation hours to guarantee safety and availability of the future reactor. In our studies we use ultraviolet femtosecond laser pulses to analyze tungsten (W) tiles that were exposed to a deuterium plasma in the linear plasma device PSI-2, which mimics conditions at the first wall. A high-resolution spectrometer is used to detect the Balmer-α transition of the surface from implanted hydrogen isotopes (H and D). We use Calibration Free CF-LIBS to quantify the amount of deuterium stored in W. This proof-of-principle study shows the applicability of femtosecond lasers for the detection of low deuterium concentration as present in first wall material of prevailing fusion experiments.

The Plasma-Facing Components (PFCs) of a magnetically confined fusion vacuum chamber are exposed to extreme environmental conditions including extraordinary high temperature, radiation, and high energy particle fluxes. All those circumstances will lead to surface erosion, particle deposition, and potentially destruction with a resulting higher likelihood of fuel retention during the fusion-plasma operation[1–3]. To ensure the safety and tritium self-sufficiency of an upcoming fusion reactor, the total absorbed amount of deuterium and tritium inside of the PFCs need to be tracked in-situ over many operation hours. The use of Laser-Induced Breakdown Spectroscopy (LIBS) has been proposed[4], as it has also numerous applications in hands-off, low invasive diagnostics like nuclear waste management[5] or material analysis in current and upcoming mars missions[6]. Especially, when it comes to the detection of minor elements and high depth resolution applications, LIBS appears as a powerful tool[7–9]. One requirement for a quantitative LIBS method is a reduced heat diffusion to the bulk material by the laser pulses so that stoichometric approximations might hold, when the expanding plasma is analyzed. To ensure this and to achieve a high depth resolution, the use of a laser pulse duration shorter than picoseconds is a preferred solution[10].

In this work we used UV ultra-short laser pulses for laser plasma generation in an argon environment, coupled with optical emission detection with a high spectral resolution Czerny-Turner spectrometer. The detection method here is similar to studies by Kurniawan et al.[11]. This system capabilities combined with a CF-LIBS approach allowed detection and quantification of the hydrogen and deuterium content of tungsten tiles exposed to a deuterium plasma in the linear plasma device PSI-2 at Forschungszentrum Jülich[12]. These tiles serve as surrogates for PFCs in this context. The deuterium content calculated with CF-LIBS was directly compared to results obtained with Thermal Desorption Spectroscopy (TDS). The UV wavelength of 343 nm and the pulse duration of 500 fs were chosen to work towards the highest possible depth resolution, which is promising due to the small optical penetration depth of 7.4 nm in tungsten[13]. This work serves as a proof-of-principle for in-situ quantification of isotopes of hydrogen for future application in plasma-facing components in confinement fusion experiments.

Results and discussion

The following experiments are executed with the setup described in detail in the methods section. Here, an argon gas flow, according to similar findings[14], is used to enhance the observed plasma emission. The heavier Ar atoms in the ambient gas (compared to nitrogen atoms in air) around the expanding plasma lead to a longer plasma persistence. This and a higher plasma temperature lead to stronger line emission. Figure 1 presents the temporal evolution of the emission of neutral tungsten (W-I at 643.97 nm) and hydrogen Balmer-α (H_α at 656.28 nm) from the tiles surface using air and an argon flow in the ambient atmosphere. We observe an increase in half-life of

[1]Institute of Laser and Plasma Physics, Heinrich-Heine University Düsseldorf, 40225 Düsseldorf, Germany. [2]Laser Technologies Group, Lawrence Berkeley National Laboratory, Berkeley, CA 94720, USA. [3]Forschungszentrum Jülich GmbH IEK-4 Plasmaphysik, 52425 Jülich, Germany. [4]Department of Mechanical Engineering, University of California at Berkeley, Berkeley, CA 94720-1740, USA. ✉email: steffen.mittelmann@hhu.de

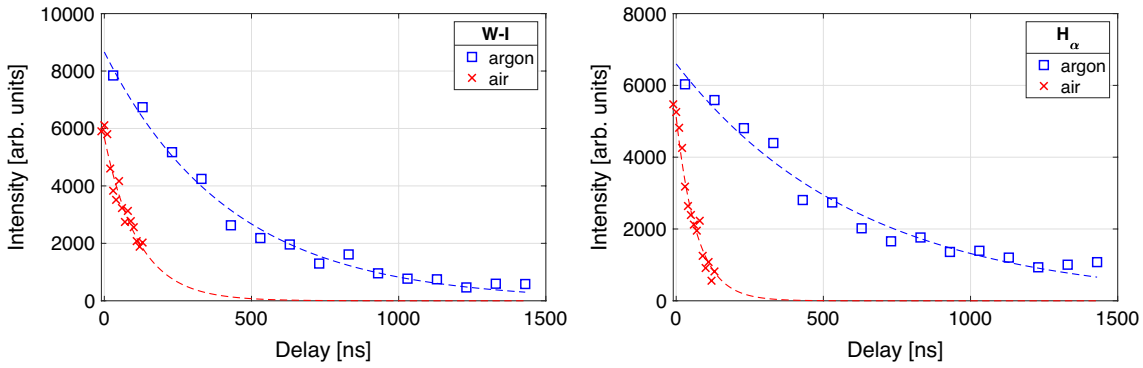

Figure 1. Detected maximum count (gate width 100 ns) of the W-I (left) and H_α (right) spectral lines at 643.97 nm and 656.28 nm on untreated tungsten (W) tile using the same setup with ambient argon (blue squares) and air (red crosses) at atmospheric pressure. Exponential fits are indicated with dashed lines.

more than a factor of two. This results in a significant signal enhancement. The electron number density n_e and heavy particle temperature T_h in the plasma are determined by observing the H_α peak. The FWHA (Full Width at Half Area) line broadening contains information on n_e using equation (5) and the Doppler width (4) is used to determine T_h. This temperature can be compared to the electron temperature in the plasma T_e determined by the Boltzmann-plot method. In Local Thermodynamic Equilibrium (LTE) conditions these temperatures can be assumed to be equal $T_h = T_e = T$.

Before we discuss the experimental requirements that are necessary to observe the deuterium impact on the exposed tungsten tiles, the temporal optical emission of the laser-induced plasma in this experiment is presented using a laser fluence of 31 J/cm^2. This value is significantly above the ablation threshold of tungsten $F_{th} = (0.07 \pm 0.06)$ J/cm^2, determined according widely applied procedure[13,15–17]. Figure 2 shows the temporal evolution of the spectra observed in this configuration with a spectrometer of instrumental broadening $w_{inst} = 52$ pm (Gaussian width) at a slit size of 100 μm. Here, the instrumental broadening of the used device is determined by the spectral lines widths of a low pressure iron (Fe) Hollow Cathode Lamp (HCL). The spectral lines used for the Boltzmann-plot method are given in table 1.

Moreover, we can observe several atomic tungsten lines and the hydrogen Balmer-α transition (H_α). The temperatures, calculated using the Boltzmann-plot method and the Doppler Broadening, similar to other recent evaluations of LIBS data[19–21], are given in Fig. 3 (left) for gate delays larger than 400 ns. The electron number density is evaluated by observing the FWHA of the H_α line and is exponentially decreasing from 2.5×10^{17} cm^{-3} by one order of magnitude in the first 800 ns as shown in Fig. 3 (right). Note that the observed hydrogen Balmer-α line interferes with a tungsten line at 656.32 nm and the weak signal from the low concentration deuterium D_α at 656.1 nm. Most likely, the pseudo-Voigt fit is influenced by these disturbances and the calculated temperature and density values may be overestimated.

Summing up the result of the plasma observation from the given material, the plasma temperature and number density decreases with time as expected. The parameters are in the range of $T_e \approx 15,000$ K to $T_e \approx 10,000$ K (Boltzmann-plot method) and $n_e \approx 2.5 \times 10^{17}$ cm^{-3} to $n_e \approx 10^{16}$ cm^{-3}. Note that the evaluated temperatures for delays lower than 400 ns are strongly deviating from reasonable values, that is why they are not plotted here. One reason for this is the high plasma density in the early expansion phase that brings a higher self-absorption and effects like opacity broadening[22] leading to an overestimation of the spectral width of the hydrogen emission. Another explanation might be given by the differences in the first ionization potential of tungsten (7.86 eV) and hydrogen (13.598 eV) that influences the atom to ion proportion according to the Saha equation. As an

Species	λ_{ki}[nm]	A_{ki}[s^{-1}]	Acc. (%)	g_k	E_k[eV]
W-I	484.381	1.9×10^6	< 10	5	2.97
W-I	488.6899	8.1×10^5	< 10	11	3.31
W-I	500.6150	1.2×10^6	< 10	7	3.25
W-I	501.5304	5.4×10^5	< 10	9	3.07
W-I	643.970	1.29×10^5	≤ 25	9	4.71
H_α	656.28	4.41×10^7	≤ 0.3	18	12.09
D_α	656.10	4.41×10^7	≤ 1	18	12.09

Table 1. Spectroscopic parameters of lines selected from atomic tungsten (W-I) and the hydrogen isotope lines (H_α, D_α) taken from the atomic spectra database NIST[18]. Here, the transition wavelength λ_{ki} from the upper energy level E_k are given with the corresponding transition probabilities A_{ki} and statistical weights g_k including the corresponding accuracy.

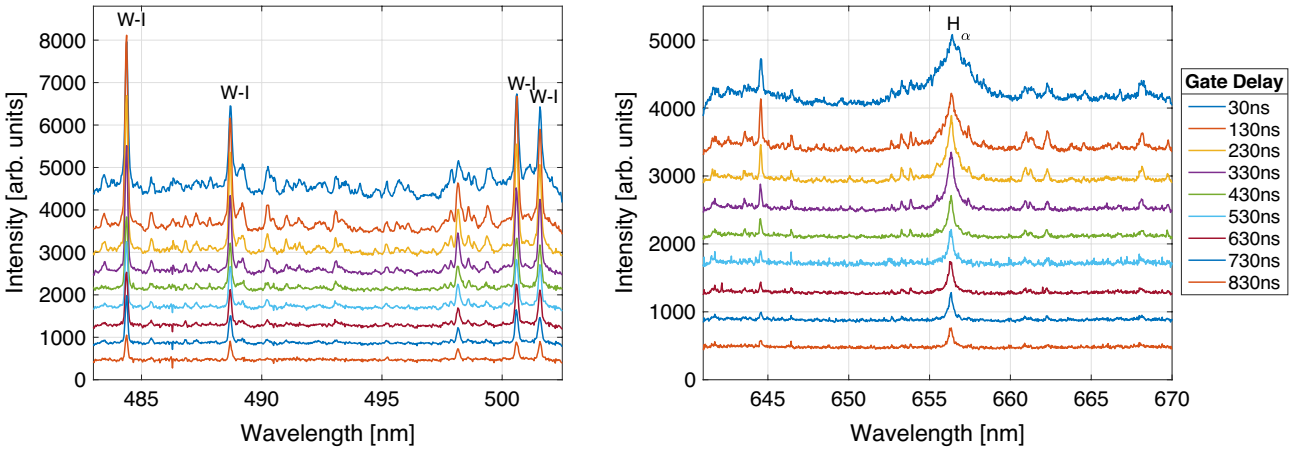

Figure 2. Time resolved emission from the tungsten sample under fs laser irradiation in argon. The gate width is set to 100 ns and the laser fluence is determined as 31 J/cm^2. For visibility 400 counts are added across two distinct spectral ranges for each given gate delay.

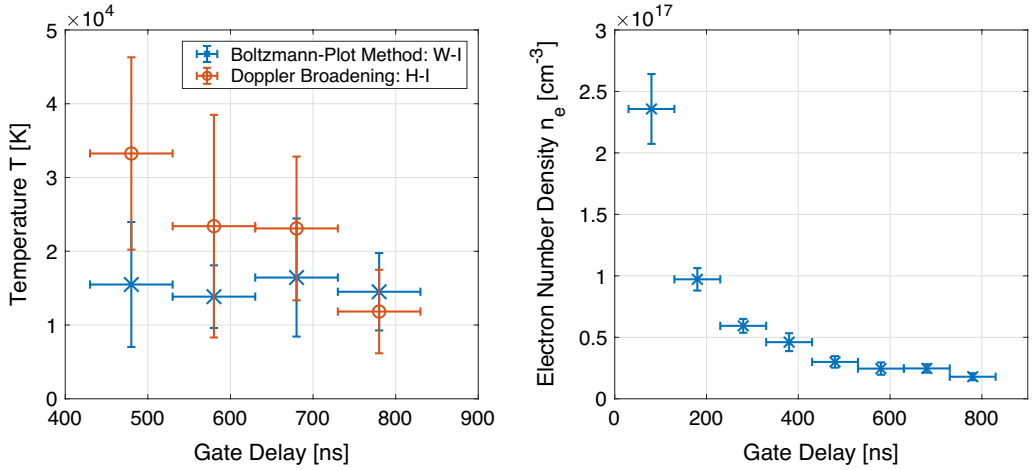

Figure 3. Left: Plasma temperature T evaluated from the observed tungsten (W) spectrum by using the Bolzmann-plot method including atomic W-I lines in blue crosses and the Doppler Broadening of the H_α line in orange circles. Right: Electron number density n_e evaluated by Stark broadening of the same line. Error-bars indicate statistical deviations from the measured values on the y-axis and the used gate width on the x-axis.

example, the ionization rate N_{ion}/N_{tot} is significantly higher for tungsten (factor 20) with $T \approx 12,000$ K and $n_e \approx 10^{17}\,\mathrm{cm}^{-3}$. Similar observations were made by Giacomo et al. (2008)[23] who observed the hydrogen emission in an aluminum plasma. The higher influence of the continuum radiation can also be observed in this regime, as well as a high plasma speed that can lead to blue shifts, slight broadening, and line asymmetry. Hence, the plasma parameters observed after 400 ns are typical values for laser-induced plasmas in an argon environment[24]. One important takeaway from the presented measurement is the transient character of the plasma observed by the exponential decrease of the number density. This is also the critical point that has to be considered, when we apply a LTE to the observed plasma. The question is whether the relaxation time τ_{rel} and corresponding diffusion length $\lambda = (D_h \cdot \tau_{rel})^{1/2}$ can be covered[25]. Here, D_h is the material dependent diffusion coefficient. Typical values for metals are on the order of $\tau_{rel} \sim 10^{-9}$ s and $\lambda \sim 10^{-5}$ m. The plasma persistence (about a few micro seconds) and plasma size (even larger than the beam diameter $\sim 20\,\mu$m) of the observed expansion suggests that a LTE is reasonable in the recombination part of the process. Moreover, the McWhirter criterion in Eq. (2) is a necessary but not sufficient condition to be fulfilled. As an example it is calculated for the tungsten plasma observed with a delay of 830 ns: $T_e \approx 10,000$ K, $n_e \approx 4.7 \times 10^{16}\,\mathrm{cm}^{-3}$ and $\Delta E_{mn} \approx 3$ eV fulfills the condition as $n_e > 4.3 \times 10^{15}\,\mathrm{cm}^{-3}$.

With this knowledge about the process, we proceeded with the detection and evaluation of the hydrogen Balmer-α transition from the tungsten tile with the high resolution spectrometer (instrumental broadening $w_{inst} = 12.7$ pm at slit width of 120 μm determined by a deuterium lamp). In Fig. 4 the detected LIBS signals of a tungsten tile exposed to the deuterium plasma in PSI-2 as in Jiang et al. (2021)[12] is compared to an unexposed tile. In blue the accumulated LIBS emission data from 80 independent single pulse interactions on the unperturbed sample surfaces are plotted and in orange the sum of all measurements from laser pulse number 2 to 5 on the

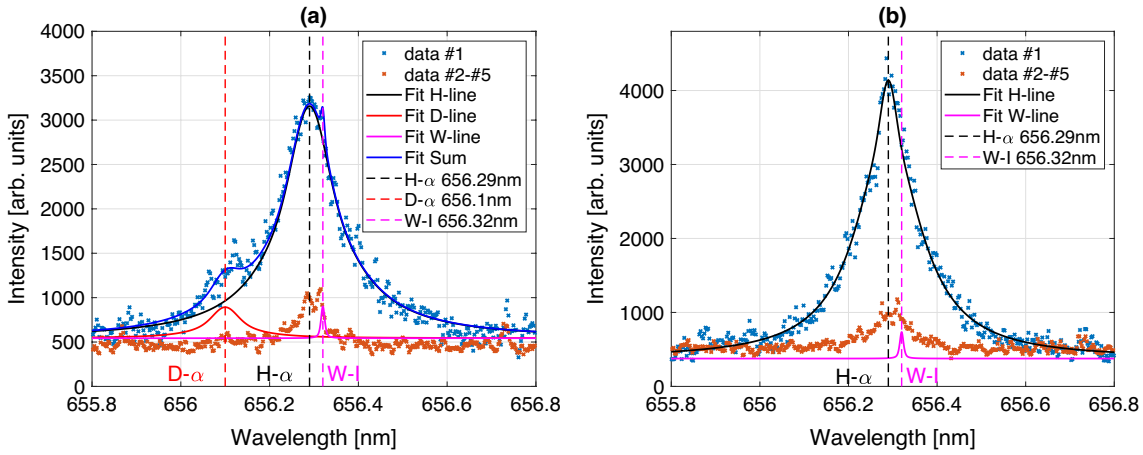

Figure 4. Left: High resolution detection of hydrogen isotope lines (H_α and D_α) in the exposed tungsten tile. Right: Comparable record on a pure tungsten tile. In black, red, and blue pseudo-Voigt fits of the overlapping deuterium and hydrogen spectral line of Balmer-α transition are given. The blue crosses represent the measurement of the first laser pulse (average of 80 positions) and orange the second to fifth pulse at the same positions respectively. Colored in magenta the neutral W-I line at 656.32 nm with fixed width and amplitude is given. The applied gate delay and width are chosen as 1.08 μs.

same positions. First of all, a distinct deuterium line at 656.1 nm is detected in the exposed tile (left), while in the unexposed tile (right) only the hydrogen line at 656.28 nm can be observed. The presence of the hydrogen line in both tiles is most likely attributed to adsorbed moisture on the surface and hydrogen remaining in the bulk. Moreover, it is important to point out that after the first laser pulse no Balmer-α line can be detected. Only the atomic tungsten line at 656.32 nm can be observed. Applying a pseudo-Voigt fit of the superposition of H_α, D_α and the W-I line allows us to compare the broadening effects on the heavy and regular hydrogen atoms. Here, we observe FWHM of $\Delta\lambda_H = 231$ pm and $\Delta\lambda_D = 140$ pm respectively. This discrepancy can be explained by different reduced masses μ of the collision partners influencing the Stark effect and the dependency of the Doppler width on the atomic mass as $\sim \sqrt{m^{-1}}$. It is known that combination of collision and temperature effects are responsible for the line broadening[26].

Observing the corresponding crater for this LIBS measurement provides information on the possible ablation rate that can be applied to this setup. Figure 5 shows a typical crater produced by five single laser pulses in argon environment on the W-tile. We find that the ablation depth per pulse (depth resolution) that allows us to observe signals from low-level hydrogen and deuterium concentration is 600 nm. In this configuration the laser beam diameter D_0 is given as 20 µm. Integration over the whole crater brings the total ablated volume of (282 ± 25) µm^3 for five consecutive laser pulses.

The combination of all presented data on the temporal plasma emission dynamics and the possibility to separate the hydrogen isotopes in the first laser pulse gives us the opportunity to estimate the deuterium impact to the ablation yield. Here, a quantitative investigation on the deposition is possible and given for the tungsten tiles.

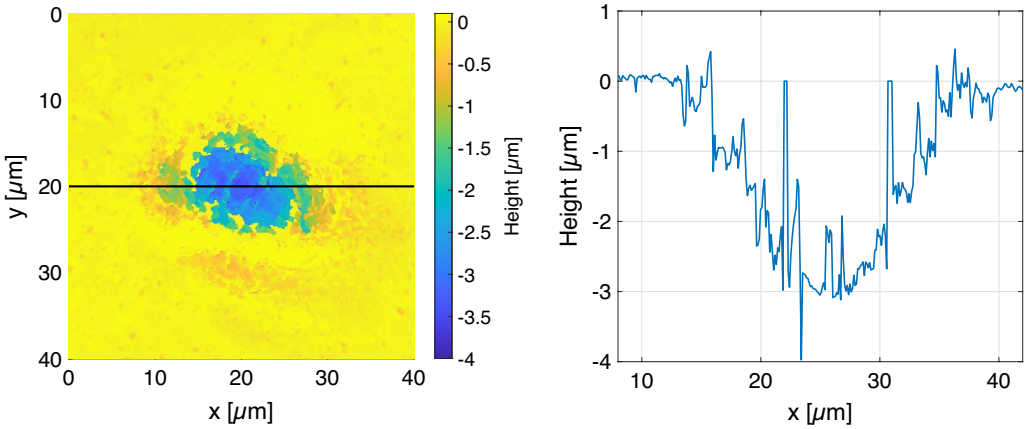

Figure 5. Left: Height map measurement with a white light interferometer to analyse the crater shape of five pulses on the same position on the W tile. The crater area is shown as a pseudo color surface plot. Right: Lineout in the center (along the black line) of the crater.

The measured temperature can be used to calculate the deuterium and hydrogen concentration by plotting the measured intensity of the hydrogen Balmer-α line to the Boltzmann-plot from equation (3). Here, it is assumed that the tungsten and hydrogen subsystems exhibit the same temperature calculated by the Boltzmann-plot method. The used spectral characteristics of the H_α line are presented in Table 1. Note that the measured intensity needs to be adapted to the sensor sensitivity calibrated by a halogen lamp of defined emission characteristics. The estimations for CF-LIBS mentioned in the methods section are applied to the calculation. In addition, the composition of the observed plasma in a LTE (delays longer than 400 ns) is assumed to be purely tungsten, hydrogen and deuterium atoms. Further impurities on the surface and in the bulk, and the argon atmosphere are ignored. From the intercept of the Boltzmann-plot the concentration of tungsten C_W and both hydrogen isotopes H and D combined $C_{H\&D}$ can be estimated. The evaluated fraction is given as

$$\%(\mathrm{H}+\mathrm{D}) = \frac{C_{H\&D}}{C_{H\&D}+C_W} \cdot 100\,\%. \tag{1}$$

From the high spectral resolution measurement in Fig. 4 and the pseudo-Voigt fits, a ratio of the integrated peak-areas is calculated as $D_\alpha/H_\alpha \approx 0.08$. This relation is transferred to the total number ratio of deuterium and hydrogen atoms N_D/N_H and can then be used to estimate the total deuterium concentration. With a total ablated volume of $(57 \pm 5)\,\mu m^3$ per laser pulse, as estimated from the findings in Fig. 5, the total number of ablated tungsten atoms is calculated as $N_W = (3.6 \pm 0.3) \times 10^{12}$. Taking into account the molar volume of tungsten as $M_{V,W} = 9.47 \times 10^{-6}\,m^3 mol^{-1}$ and applying Eq. (1), the found concentration values and the total number ratio, the number of hydrogen and deuterium atoms were calculated as $N_H = (7.8 \pm 3.9) \times 10^{11}$ and $N_D = (6.2 \pm 2.8) \times 10^{10}$ respectively, as average values determined by the detected spectra with delay $>$ 400 ns. Here, the uncertainties are just statistical variations and have to be extended by the mentioned approximations and deviations of the ablated volume. This includes that the value is probably more an upper limit due to the overestimated Balmer-α intensity that is influenced by a W-I line. Considering this, the value holds up to a comparison to the TDS data. The total number of deuterium atoms detected in the whole sample is estimated as $(3.8 \pm 0.8) \times 10^{16}$. Here, an accuracy of around 21% is calculated. From this we expect up to $(1.2 \pm 0.2) \times 10^{11}$ atoms on the laser irradiated spot in the LIBS experiment, which is a factor two larger than what we calculated by the CF-LIBS approach. This deviation might result from the uncertainty of the two methods, as it can be expected from studies on PSI-2[27] that deuterium is only stored in depths of around 100 nm. Also note that the deuterium distribution along one dimension of the tiles surface is not homogeneous due to the plasma gradient given in the exposure process. This can result in an over or underestimation of the expected deuterium number depending on the position on the tile. The presented measurement is executed close to the center of the tile and along the axis where we do not expect significant changes in the deposition. In conclusion, the presented CF-LIBS method can be used to determine the deuterium impact in the used W tiles as around (1.7 ± 0.5) at% in the first 600 nm behind the surface with a high lateral resolution of $\sim 20\,\mu m$, according to the crater diameter.

Conclusion

We demonstrated the use of femtosecond UV LIBS as a prospect high depth resolution diagnostic technique to analyze the hydrogen isotope impurities in metallic samples that are used as PFCs in confinement fusion experiments. With an ablation rate of 600 nm per pulse, deuterium and hydrogen can be detected with this method. Here the limitation of femtosecond LIBS can be observed compared to studies with picosecond lasers that provide a higher pulse energy. In particular, the studies by Oelmann et al. (2021)[28] exhibit a depth resolution of 30 nm in a double-pulse configuration. With an enormously shorter heat entry to the sample the heat affection by the laser is smaller and desorption of light particles from higher depths is less likely in relation to ns-LIBS experiments. This will influence quantitative approaches like Xing et al.[29], because the ablated volume can not be consulted to calculate the deposited deuterium fraction. The applied CF-LIBS method here is an interesting quantitative approach to estimate the total deuterium content in the investigated tungsten tiles and is even more significant due to the use of the femtosecond laser to provide a reasonable depth and high lateral resolution. The estimated deuterium content of approximately 1.7 at% using this method is close to the expected quantity in the tungsten tiles that were exposed to deuterium plasma. Moreover, similar concentrations of hydrogen retention was found like in the comparable study by Pardede et al.[30]. Further studies on this approach with tiles of varying deuterium content would be the next logical step to develop this method and to determine the limit of detection. In addition, interesting approaches to enhance the detected plasma emission will be beneficial to improve the signal-to-noise ratio[31]. In conclusion, this work provides insights into the use of all-optical laser plasma techniques for future in-situ analysis of plasma-facing components in fusion applications.

Methods

In the following, the used experimental setup, evaluation methods, and sample preparation techniques are described. For more details on the determination of ablation threshold fluence of tungsten, and the results from the fitting function, refer to the provided supplemental information.

Experimental setup. The basic setup of the LIBS experiment is shown in Fig. 6. It consists of a $\lambda = 1030$ nm, 500 fs laser in single pulse mode and a setup for second and third harmonic generation. In this set of experiments, the third harmonic of the fundamental laser frequency was used at 343 nm. The generated pulses with an output pulse energy of up to 100 μJ are focused by a 3x objective lens (working distance 50 mm) to the target placed in an experimental cell (10 cm $\times$ 10 cm $\times$ 5 cm) that can be filled with different gas compositions from an external inlet. Here an argon gas flow of 2 l/min is chosen to change the environmental conditions. The

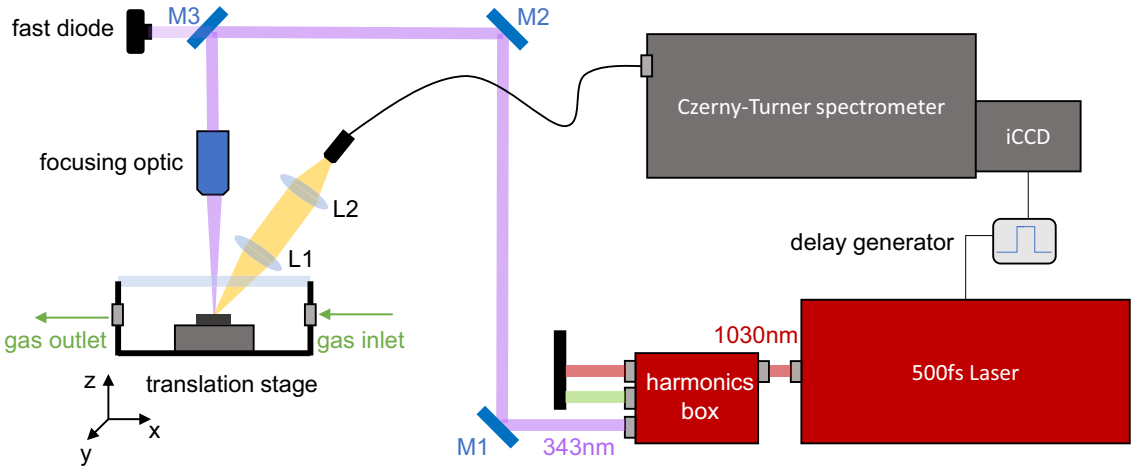

Figure 6. Experimental Setup of femtosecond UV LIBS experiment including the laser system, harmonic generation box, a set of mirrors (M1-M3), the focusing optic, a translation stage with the sample inside of a chamber with a gas in- and outlet, and the collection system with two lenses (L1 and L2) and a Czerny-Turner spectrometer with iCCD camera.

whole cell is placed on motorized stages to control the distance between the focusing lens and the target and to irradiate different positions on the surface. A collection system consists of two plano-convex fused silica lenses ($f_1 = 50$ mm and $f_2 = 100$ mm) and an optical fiber that is coupled to the setup to collect the plasma radiation and image it to the entrance slit of a Czerny-Turner spectrometer. The plasma emission signal is detected by an iCCD camera.

In this work, we studied the time resolved UV femtosecond LIBS emission from tungsten tiles that were exposed to a deuterium plasma in a linear plasma device, and followed by the detection and quantification of the hydrogen isotopes in these samples.

Preparation of W-tiles. The material under investigation is pure polished tungsten (W, $Z = 74$) with a surface roughness of $S_a = 60$ nm. The tiles (9.9 mm × 9.9 mm × 5.1 mm) are baked out under 1000 °C for three hours and exposed to deuterium in the linear plasma device PSI-2 at Forschungszentrum Jülich. The tiles are arranged in a circle on a molybdenum mask while the ring shaped plasma interacts with it. Plasma parameters are detected by a Langmuir probe frequently during the four hour process. The maximum deuterium flux is measured as 2.9×10^{21} m^{-2}s^{-1} with a total fluence of 3×10^{25} m^{-2} onto the tile surface heated to a temperature of 230 °C. The plasma parameters in the PSI-2 to mimic the fusion plasma are described by Kreter et al.[27]. From this overview, a deuterium concentration of up to 2 at% in the first 1 µm behind the surface is reasonable with the used settings. According to a Thermal Desorption Spectroscopy (TDS) measurement applied ex-situ after the exposure, the total number of detected deuterium atoms deposited per area in the bulk are given as $N_D = (3.9 \pm 0.8) \times 10^{20}$ m^{-2}, and $N_H = (4.1 \pm 1.1) \times 10^{21}$ m^{-2} hydrogen atoms. The ratio of N_D to N_H is with 0.095 close to the calculated value from the high resolution LIBS experiment.

Evaluation of the results. In this section we give an overview of the used methods to evaluate the measured spectra and how to gain more information from the samples under investigation. Calculations of plasma parameters such as temperature and electron number density are necessary to resolve a spectrum from hydrogen and deuterium impurities in the used metal tiles. Cristoforetti et al.[25] showed that the expanding, transient plasma created by the laser pulse and interacting with the ambient gas can be in a LTE under certain circumstances. This state is a necessary condition to make predictions on the plasma parameters. Following the conditions formulated there and the criterion given by McWhirter et al.[32],

$$n_e > 1.6 \times 10^{12} (T[\mathrm{K}])^{1/2} (\Delta E_{mn}[\mathrm{eV}])^3, \tag{2}$$

the tenability of this state is reviewed. Note that the McWhirter criterion alone is not sufficient in this context.

The acceptance of a LTE allows the application of the Saha equation and a Maxwellian velocity distribution on the electrons in the expanding plasma. Moreover, this implies that the temperature of electrons and all other particles in the plasma plume are equal ($T_e = T_h$) and we want to assumed that it is optically thin. In this case we can apply the linear form of the Boltzmann-plot method as

$$\ln\left(\frac{\lambda_{ki} I_{ki}}{h c A_{ki} g_k}\right) = -\frac{E_k}{k_B T} + \ln\left(\frac{F C_s}{U_s(T)}\right). \tag{3}$$

In this equation the indices k and i represent the upper and lower state of the excited species respectively, the natural constants are given as h for Planck, k_B for Boltzmann and c for the vacuum light velocity. Additional parameters for the transition wavelength λ_{ki} like transition probability A_{ki}, statistical weight g_k, and upper

energy level E_k can be extracted from common literature (e.g. NIST library[18]). $U_s(T)$ is the temperature dependent partition function that can be calculated according to the statistical weight and energy levels given for each material from the same library. Note that the experimental factor F is the same for all analyzed materials in the same plasma as it depends on the collection system and plasma size. The linear character ($y = mx + q_s$) of this form allows the extraction of the temperature value from the slope $m = -(k_B T)^{-1}$ by plotting the data on a logarithmic axis. In the intercept we can find the information on the species concentration C_s to the extend of the experimental factor F. This fact can be used in a Calibration Free LIBS method (CF-LIBS) to estimate the amount of ablated deuterium in the detected plasma matrix. The application of this is discussed in detail in the experimental result section. For now we assume that the ablated material contribution can be mapped by the spectral emission distribution. Specifically, we work under the assumption of stoichiometric ablation[33,34], that the observed plasmas (in a reasonable time frame) are optically thin, and that the used spectral lines for the Boltzmann-plot method are not self-absorbing.

The evaluation of the electron number density is made by analysis of the spectral line broadening of the hydrogen Balmer-α emission. The spectral line shape is determined by the convolution of different effects, where natural line broadening and van-der-Waals broadening are neglected and the instrumental broadening is determined for every measurement. The two dominant effects are the Doppler broadening, which is a temperature effect, and the Stark broadening induced by collisions of the charged particles, especially electrons, with the other parts present in the plasma. Due to the assumed Maxwell-Boltzmann velocity distribution the spectral lines are influenced by the plasma temperature and a Gaussian shape of width

$$w_{Doppler} = \frac{\lambda_0}{c}\sqrt{2\ln 2\frac{k_B T}{m_s}}, \tag{4}$$

with spectral line wavelength λ_0 and species mass m_s, can be observed. This width is given as the full width at half maximum (FWHM) divided by the factor $2\sqrt{2\ln 2}$. The Stark broadening follows a Lorentz profile and the electron number density n_e can be estimated by the half width w_{Stark}, also called Stark width, and the Stark broadening parameter w_0 that can be found in literature. Note that w_0 also depends on the plasma temperature. It has been shown in[35,36] that it is possible to neglect the temperature dependence by determining the Half Width at Half Area (HWHA) of the deconvoluted Lorentz part of the Balmer-α emission line and calculate n_e by

$$\mathrm{HWHA[nm]} = 0.549 \cdot \left(\frac{n_e[\mathrm{cm}^{-3}]}{10^{17}}\right)^{0.67965}. \tag{5}$$

Taking into account the convolution of the Gaussian and the Lorentz shape, a pseudo-Voigt fit as described in[37] is used in this contribution to extract the plasma parameter from the line shape characteristic. We found that this fitting method was significantly more stable in the data processing compared to a real Voigt fit, also with data sets of lower signal-to-noise ratio. More information on the fitting function can be found in the SI.

Data Availability

The experimental datasets generated during the current study are available from the corresponding author on reasonable request.

Received: 7 November 2022; Accepted: 31 January 2023
Published online: 09 February 2023

References

1. Roth, J. *et al.* Tritium inventory in ITER plasma-facing materials and tritium removal procedures. *Plasma Phys. Controlled Fusion* **50**, 103001. https://doi.org/10.1088/0741-3335/50/10/103001 (2008).
2. Brezinsek, S. *et al.* Beryllium migration in JET ITER-like wall plasmas. *Nucl. Fusion* **55**, 063021. https://doi.org/10.1088/0029-5515/55/6/063021 (2015).
3. Maurya, G. S., Marín-Roldán, A., Veis, P., Pathak, A. K. & Sen, P. A review of the LIBS analysis for the plasma-facing components diagnostics. *J. Nucl. Mater.* **541**, 152417. https://doi.org/10.1016/j.jnucmat.2020.152417 (2020).
4. Huber, A. *et al.* Development of laser-based diagnostics for surface characterisation of wall components in fusion devices. *Fusion Eng. Des.* **86**, 1336–1340. https://doi.org/10.1016/j.fusengdes.2011.01.090 (2011).
5. Chan, G.C.-Y. *et al.* Analytical characterization of laser induced plasmas towards uranium isotopic analysis in gaseous uranium hexafluoride. *Spectrochim. Acta Part B* **176**, 106036. https://doi.org/10.1016/j.sab.2020.106036 (2021).
6. McCanta, M., Dobosh, P., Dyar, M. & Newsom, H. Testing the veracity of LIBS analyses on mars using the LIBSSIM program. *Planet. Space Sci.* **81**, 48–54. https://doi.org/10.1016/j.pss.2013.03.004 (2013).
7. Heikkilä, P., Rostedt, A., Toivonen, J. & Keskinen, J. Elemental analysis of single ambient aerosol particles using laser-induced breakdown spectroscopy. *Sci. Rep.* **12**, 1–9. https://doi.org/10.1038/s41598-022-18349-8 (2022).
8. Chirinos, J. R. *et al.* Simultaneous 3-dimensional elemental imaging with LIBS and LA-ICP-MS. *J. Anal. At. Spectrom.* **29**, 1292–1298. https://doi.org/10.1039/C4JA00066H (2014).
9. Lu, Y., Zorba, V., Mao, X., Zheng, R. & Russo, R. E. UV fs-ns double-pulse laser induced breakdown spectroscopy for high spatial resolution chemical analysis. *J. Anal. At. Spectrom.* **28**, 743–748. https://doi.org/10.1039/C3JA30315B (2013).
10. Le Harzic, R. *et al.* Comparison of heat-affected zones due to nanosecond and femtosecond laser pulses using transmission electronic microscopy. *Appl. Phys. Lett.* **80**, 3886–3888. https://doi.org/10.1063/1.1481195 (2002).
11. Kurniawan, K. H. & Kagawa, K. Hydrogen and deuterium analysis using laser-induced plasma spectroscopy. *Appl. Spectrosc. Rev.* **41**, 99–130. https://doi.org/10.1080/05704920500510687 (2006).
12. Jiang, X., Sergienko, G., Kreter, A., Brezinsek, S. & Linsmeier, C. In situ study of short-term retention of deuterium in tungsten during and after plasma exposure in psi-2. *Nucl. Fusion* **61**, 096006. https://doi.org/10.1088/1741-4326/ac112e (2021).
13. Werner, W. S., Glantschnig, K. & Ambrosch-Draxl, C. Optical constants and inelastic electron-scattering data for 17 elemental metals. *J. Phys. Chem. Ref. Data* **38**, 1013–1092. https://doi.org/10.1063/1.3243762 (2009).

14. Hermann, J. *et al.* Ideal radiation source for plasma spectroscopy generated by laser ablation. *Phys. Rev. E* **96**, 053210. https://doi.org/10.1103/PhysRevE.96.053210 (2017).
15. Mittelmann, S. *et al.* Laser-induced ablation of tantalum in a wide range of pulse durations. *Appl. Phys. A* **126**, 1–7. https://doi.org/10.1007/s00339-020-03838-2 (2020).
16. Chichkov, B. N., Momma, C., Nolte, S., Von Alvensleben, F. & Tünnermann, A. Femtosecond, picosecond and nanosecond laser ablation of solids. *Appl. Phys. A* **63**, 109–115. https://doi.org/10.1007/BF01567637 (1996).
17. Lickschat, P., Metzner, D. & Weißmantel, S. Fundamental investigations of ultrashort pulsed laser ablation on stainless steel and cemented tungsten carbide. *Int. J. Adv. Manuf. Technol.* **109**, 1167–1175. https://doi.org/10.1007/s00170-020-05502-8 (2020).
18. Kramida, A., Ralchenko, Y., Reader, J. & Team, N. A. Nist atomic spectra database (ver. 5.9). https://doi.org/10.18434/T4W30F(2021).
19. Dwivedi, V. *et al.* CF-LIBS study of pure ta, and WTa+ D coating as fusion-relevant materials: a step towards future in situ compositional quantification at atmospheric pressure. *Eur. Phys. J. Plus* **136**, 1177. https://doi.org/10.1140/epjp/s13360-021-02179-0 (2021).
20. Mal, E., Junjuri, R., Gundawar, M. K. & Khare, A. Temporal characterization of laser-induced plasma of tungsten in air. *Laser Part. Beams* **38**, 14–24. https://doi.org/10.1017/S0263034619000788 (2020).
21. Russo, R. E., Mao, X., Gonzalez, J. J., Zorba, V. & Yoo, J. Laser ablation in analytical chemistry. *Anal. Chem.* **85**, 6162–6177. https://doi.org/10.1021/ac4005327 (2013).
22. Hacar, A., Alves, J., Burkert, A. & Goldsmith, P. Opacity broadening and interpretation of suprathermal co linewidths: Macroscopic turbulence and tangled molecular clouds. *Astron. Astrophys.* **591**, A104. https://doi.org/10.1051/0004-6361/201527319 (2016).
23. De Giacomo, A. *et al.* Spatial distribution of hydrogen and other emitters in aluminum laser-induced plasma in air and consequences on spatially integrated laser-induced breakdown spectroscopy measurements. *Spectrochim. Acta Part B* **63**, 980–987. https://doi.org/10.1016/j.sab.2008.06.010 (2008).
24. Aragón, C. & Aguilera, J. A. Characterization of laser induced plasmas by optical emission spectroscopy: A review of experiments and methods. *Spectrochim. Acta Part B* **63**, 893–916. https://doi.org/10.1016/j.sab.2008.05.010 (2008).
25. Cristoforetti, G. *et al.* Local thermodynamic equilibrium in laser-induced breakdown spectroscopy: Beyond the McWhirter criterion. *Spectrochim. Acta Part B* **65**, 86–95. https://doi.org/10.1016/j.sab.2009.11.005 (2010).
26. Zhang, S. *et al.* Laser-induced plasma temperature. *Spectrochim. Acta Part B* **97**, 13–33. https://doi.org/10.1016/j.sab.2014.04.009 (2014).
27. Kreter, A. *et al.* Influence of plasma impurities on the fuel retention in tungsten. *Nucl. Fusion* **59**, 086029. https://doi.org/10.1088/1741-4326/ab235d (2019).
28. Oelmann, J., Wüst, E., Sergienko, G. & Brezinsek, S. Double pulse laser-induced breakdown spectroscopy for the analysis of plasma-facing components. *Phys. Scr.* **96**, 124064. https://doi.org/10.1088/1402-4896/ac379c (2021).
29. Xing, Y. *et al.* Quantitative analysis of hydrogen isotopes in hydrogen storage material using laser-induced breakdown spectroscopy. *Nucl. Mater. Energy* **31**, 101204. https://doi.org/10.1016/j.nme.2022.101204 (2022).
30. Pardede, M. *et al.* High sensitivity hydrogen analysis in zircaloy-4 using helium-assisted excitation laser-induced breakdown spectroscopy. *Sci. Rep.* **11**, 1–10. https://doi.org/10.1038/s41598-021-01601-y (2021).
31. Yang, G., Lin, Q., Ding, Y., Tian, D. & Duan, Y. Laser induced breakdown spectroscopy based on single beam splitting and geometric configuration for effective signal enhancement. *Sci. Rep.* **5**, 1–11. https://doi.org/10.1038/srep07625 (2015).
32. Fujimoto, T. & McWhirter, R. Validity criteria for local thermodynamic equilibrium in plasma spectroscopy. *Phys. Rev. A* **42**, 6588. https://doi.org/10.1103/PhysRevA.42.6588 (1990).
33. Tognoni, E., Cristoforetti, G., Legnaioli, S. & Palleschi, V. Calibration-free laser-induced breakdown spectroscopy: State of the art. *Spectrochim. Acta Part B* **65**, 1–14. https://doi.org/10.1016/j.sab.2009.11.006 (2010).
34. Roldán, A. M., Pisarčík, M., Veis, M., Držík, M. & Veis, P. Calibration-free analysis of a tungsten-based target for diagnostics of relevant fusion materials comparing picosecond and nanosecond libs. *Spectrochim. Acta Part B* **177**, 106055. https://doi.org/10.1016/j.sab.2020.106055 (2021).
35. Gigosos, M. A., Gonzalez, M. A. & Cardenoso, V. Computer simulated Balmer-alpha,-beta and-gamma stark line profiles for non-equilibrium plasmas diagnostics. *Spectrochim. Acta Part B* **58**, 1489–1504. https://doi.org/10.1016/S0584-8547(03)00097-1 (2003).
36. Konjević, N., Ivković, M. & Sakan, N. Hydrogen Balmer lines for low electron number density plasma diagnostics. *Spectrochim. Acta Part B* **76**, 16–26. https://doi.org/10.1016/j.sab.2012.06.026 (2012).
37. Ida, T., Ando, M. & Toraya, H. Extended pseudo-Voigt function for approximating the Voigt profile. *J. Appl. Crystallogr.* **33**, 1311–1316. https://doi.org/10.1107/S0021889800010219 (2000).

Acknowledgements

We want to thank Fulbright Germany for making this cooperation possible in the context of a research exchange program. We also want to give credits to the research teams of the Laser Technologies Group at Lawrence Berkeley National Laboratory and the IEK-4 at Forschungszentrum Jülich for providing necessary equipment, expertise, sample processing, and post mortem diagnostics. Moreover, we gratefully acknowledge the financial funding by the Deutsche Forschungsgemeinschaft (No. 410415657), and the US Department of Energy, Office of Defense Nuclear Nonproliferation Research and Development under contract number DE-AC02-05CH11231 at the Lawrence Berkeley National Laboratory.

Author contributions

S.M. and V.Z. conceived the experiment. S.M. conducted the experiment, analysed the results, and was writing the manuscript. K.T., M.P., and X.M. helped to conduct the experiment. S.B. was consulted for the tile preparation. G.P. and V.Z. supervised the project. All authors discussed the results and reviewed the manuscript.

Funding

Open Access funding enabled and organized by Projekt DEAL.

Competing interests

The authors declare no competing interests.

Additional information

Supplementary Information The online version contains supplementary material available at https://doi.org/10.1038/s41598-023-29138-2.

Correspondence and requests for materials should be addressed to S.M.